This is the peer reviewed version of the following article: Lim, JY, Loy, ACM, Alhazmi, H, et al. Machine learning–assisted CO2 utilization in the catalytic dry reforming of hydrocarbons: Reaction pathways and multicriteria optimization analyses. Int J Energy Res. 2021; 1- 15, which has been published in final form at doi:10.1002/er.7565]. This article may be used for non-commercial purposes in accordance with Wiley Terms and Conditions for self-archiving.

Machine Learning assisted CO_2 utilization in the catalytic dry reforming of hydrocarbons: Reaction pathways and multi-criteria optimization analyses

Juin Yau Lim[a+], Adrian Chun Minh Loy[b,c+], Hatem Alhazmi[d], Bridgid Chin Lai Fui[e] Kin Wai Cheah[f], Martin J. Taylor[f], Georgios Kyriakou[g] and Chang Kyoo Yoo[a]*

[a]Integrated Engineering, Dept. of Environmental Science and Engineering, College of Engineering, Kyung Hee University, 1732 Deogyeong-daero, Giheung-gu, Yongin-Si, Gyeonggi-do 17104, Republic of Korea.

[b]Department of Chemical Engineering, Universiti Teknologi PETRONAS, Bandar Seri Iskandar, Malaysia.

[c]Department of Chemical Engineering, Monash University, Victoria 3800, Australia.

[d]National Center for Environmental Technology (NCET), King Abdulaziz City for Science and Technology (KACST), P.O. Box 6086, Riyadh, Saudi Arabia.

[e]Chemical and Energy Engineering, Faculty of Engineering and Science, Curtin University Malaysia, CDT 250, 98009 Miri, Sarawak, Malaysia.

[f]Energy and Environment Institute, University of Hull, Cottingham Road, Hull, HU6 7RX, United Kingdom

[g]Department of Chemical Engineering, University of Patras, Caratheodory 1, Patras GR 265 04, Greece

** Corresponding author: Tel: +82-31-201-3824; fax: +82-31-202-8854; email: ckyoo@khu.ac.kr*

[+]First and second authors contributed equally to this work

Abstract

The catalytic dry reforming (DR) process is a clean approach to transform CO_2 into H_2 and CO rich synthetic gas that can be used for various energy applications such as Fischer-Tropsch fuels production. A novel framework is proposed to determine the optimum reaction configurations and reaction pathways for DR of C_1-C_4 hydrocarbons *via* a Reaction Mechanism Generator (RMG). With the aid of machine learning, the variation of thermodynamic and microkinetic parameters based on different reaction temperatures, pressures, CH_4/CO_2 ratios and catalytic surface, Pt(111) and Ni(111), were successfully elucidated. As a result, a promising multi-criteria decision-making process, TOPSIS, was employed to identify the optimum reaction configuration with the trade-off between H_2 yield and CO_2 reduction. Notably, the optimum conditions for the DR of C_1 and C_2 hydrocarbons were 800 °C at 3 atm on Pt(111); whereas C_3 and C_4 hydrocarbons found favor at 800 °C and 2 atm on Ni(111) to attain the highest H_2 yield and CO_2 conversion. Based on the RMG-Cat (first-principle microkinetic database), the energy profile of the most selective reaction pathway network for the DR of CH_4 on Pt(111) at 3 atm and 800 °C was deducted. The activation energy (E_a) for C-H bond dissociation *via* dehydrogenation on the Pt(111) was found to be 0.60 eV, lower than that reported previously for Ni(111), Cu(111), and Co(111) surfaces. The most endothermic reaction of the CH_4 reforming process was found to be $C_3H_3^* + H_2O^* \leftrightarrow OH^* + C_3H_4$ (218.74 kJ/mol).

Keywords

CO_2 utilization; Reaction mechanism network; Machine learning; Catalytic dry reforming; Density functional theory, Hydrogen production

1. Introduction

Over the years, carbon dioxide (CO_2) has been classified as one of the main atmospheric greenhouse gases (GHGs) responsible for anthropogenic climate change. Data from the European Environment Agency (EEA) shows that CO_2 emissions from the transport sector represented more than 25% of the total European Union 28 countries' GHGs emissions in 2017 [1,2]. However, due to its abundance CO_2 has sparked renewed interest due to its low cost as a source of clean energy, allowing it to contribute to a carbon circular economy [3–5]. To achieve a meaningful impact on both the economy and the environment, carbon dioxide utilization (CDU) must be conducted instead of storage to unlock the potential for profitable industrial applications. The proper implication of CDU is capable of reaching critical global net-zero CO_2 emissions targets by 2050. CDU will allow for the production of value-added chemicals such as hydrogen, syngas, allyl alcohols, and long-chain hydrocarbons [6–8].

Among all the syngas production technologies, the catalytic CO_2 Dry Reforming (CDR) of hydrocarbons is one of the most feasible technologies to be up-scaled into the commercial-scale chemical manufacturing process as compared to its biological counterparts due to the high hydrogen purity, short reaction time, and unnecessary CO_2 downstream purification [9–11]. Besides abating and recycling the CO_2, the Dry Reforming (DR) process can be integrated into the synthesis of various chemical building blocks without complex configurations in the system [12,13]. Practically, Dry Reforming of Methane (DRM) is the most extensively investigated technology for producing syngas with a low H_2:CO ratio, which is suitable for the synthesis of oxygenated chemicals and hydrocarbons from Fischer−Tropsch synthesis [9,14,15]. Notably, DRM reaction is favored at high temperature (600-1000 ºC) and moderate pressure (1-10 atm) to achieve considerable high conversions [16]. Recently, researchers have discovered alternative ways to convert CO_2 to syngas from the economic and safety standpoints by using light C_2-C_4 hydrocarbons such as ethane, propane, and butane found in shale gas

(natural gas trapped in porous sedimentary shale rock) [17]. With the current high growth of shale gas production at ~2.7% per year, it has become a highly sought industrial petrochemical feedstock that can produce value-added chemicals [18]. Meanwhile, from the thermodynamic stoichiometric equilibrium point of view, the conversion of CO_2 (50%) in DR of C_2H_6 and C_4H_{10} can be achieved at 488 °C and 444 °C, which is ~12-15% lower than CH_4 (560 °C) [12]. Such reduction in reaction temperatures offers better flexibility in catalyst synthesis, especially the physicochemical structural tuning of the catalysts to increase their lifespan and activity.

Over the years, Reaction Mechanism Generators (RMG: version 1.0 and 2.0) have been explored and elucidated for various chemical platform reactions, not limited to modeling for biofuels [23], ketones [24], and aromatic hydrocarbons [25]. On the other hand, density functional theory (DFT), an accurate and reliable computational method, has been widely adopted in an array of homogeneity catalytic processes to investigate the characteristics and performance of catalysts at an atomic scale [18–20]. With the aid of DFT analysis, researchers can understand the following elements in-depth: (i) identify which crystalline surface(s) of the catalyst is preferred for the desirable process; (ii) identify the possible reactions that can happen on that surface, including short-lived chemical intermediates; (iii) identify the thermodynamic parameters of all the possible reactions; and (iv) elucidate the chemical molecular dynamics of adsorption of a given reactant and material [19,20]. These kinetic and thermodynamic mechanism inputs can be further incorporated into a third-party reactor software package (i.e., ASPEN Plus, Cantera, and ANSYS Fluent) to simulate the predictions for macro-variables of interest such as product composition, ignition behavior, and flame speed. Nonetheless, RMG does not require any kinetics or thermodynamic information inputs (e.g., ΔH, E_a, and ΔG) for the process or possible reaction pathways to predict the yield of potential products, in which other well-known chemical process simulation tools do such as Aspen PLUS, Aspen HYSYS and DWSIM. Recently, a group of researchers from MIT (USA) has proposed an automated

machine learning approach, RMG-Cat, which can generate microkinetic mechanisms for heterogeneous catalysis based on the ab-initio electronic structure code database [21]. In summary, RMG-Cat has the advantage while comparing towards other automated mechanism generators such as MAMOX, RNG, and XMG, especially with its astonishing effect on handling large number of species and reactions alongside wide cheminformatics libraries [22].

In the past, many different active metals have been considered and investigated in CDR systems, such as noble metals (e.g., Rh, Ru, Pt, and Pd) and non-noble metals (e.g., Ni, Co, and Cu) [23–29]. Among the active metals, Pt and Ni metal-based catalysts are the most extensively investigated for DRM due to their high performance in C-H scission and thermal stability when at high temperatures (>700 °C) [16]. Recently, Niu and their research team have synthesized an active and stable bimetallic PtNi catalyst that exhibited improved catalytic activity compared with monometallic counterparts. The bimetallic PtNi catalyst also successfully supressed the reverse water-gas shift reaction and improved the coking resistance of the catalysts which prolonged its service life during the reaction. In the similar vein, the same research team investigated the reaction mechanism of CO_2 reforming of methane to syngas over the bimetallic PtNi catalyst in a systematic DFT study. It was revealed that the bimetallic catalyst demands a higher energy requirements than the Ni(111) and Pt(111) and the dominant reaction pathway on Pt and PtNi was determined to be H-assisted CO_2 dissociation. However, to date, there is still a lack of literature in determining the reaction pathway network and for optimizing the reactions simultaneously *via a* machine learning approach, specifically for the field of CO_2 utilization. Thus, our study aims to provide an in-depth understanding on how machine learning helps in determining the thermodynamic parameters as well as the fundamentals behind microkinetic heterogeneous catalysts-reactant systems. This study could highly contribute to bridging the research gap between process optimization and microkinetic

analysis in determining the best light hydrocarbons (LHC) *via* the CDR process on Pt(111) and Ni(111) surfaces, focusing on:

- Identifying the efficiency of converting CO_2 into a clean H_2 using LHC (C_1-C_4) *via* CDR on both Pt(111) and Ni(111) surfaces.
- Evaluating the H_2 yield generated and the rate of CO_2 reduction of all LHC involved at different operational conditions.
- Determine the best-operating conditions for each LHC assisted by TOPSIS according to the trade-off between H_2 yield and CO_2 reduction.
- Determine the output variation of the CDR process from each LHC through sensitivity analysis.
- Assessing the energy profile with the possible reaction pathways and the thermodynamic parameters for the optimized conditions for the selected LHC.

2. Methodology

The well-established artificial intelligence tool: RMG-Py (version 3.0), established on python, was applied in this study to determine all the possible reaction pathways and products in the DR of C_1-C_4 hydrocarbons [30]. The operational mechanism of RMG is based on the functional groups of the driven reactants in each reaction network proposed, with a thorough search of the RMG-database for all the possible reactions and the products. A detailed description of the essential features for RMG, including species representation, thermodynamic parameter estimation, and rate-based algorithm, can be referred in Gao *et al.* [21]. This study aims to investigate all possible decarbonization reactions initiated by CO_2 and the LHC in the core model. Subsequently, species apart from the initial specification in the reaction will be considered in the core if only the reaction flux agrees. The thermochemical properties of the species that occur in the reaction at a given operating condition (temperature and pressure) are adapted from the RMG-database (version 3.0). In the circumstances where the properties are not known, Benson's group additivity and by on-the-fly semi-empirical quantum chemistry calculations will be applied to assume the respective properties [31].

As mentioned previously, ethane which is found abundantly in shale gas and methane, the significant gas component, will be used in this study [32]. Generally, two of the primary reaction pathways in CO_2 reforming were reported: (i) Syngas (CO and H_2) production with CO_2 reforming and (ii) ethylene (C_2H_4) generation *via* oxidative dehydrogenation [33]. The former reaction pathway is more favorable in this study that allows the catalytic production of H_2. Due to the DR of hydrocarbons requiring a catalyst, the RMG-Cat (currently embedded into the current version of RMG-Py) has been employed in this study to simulate the reaction which Goldsmith and West initially proposed for methane dry reforming on Ni(111) [19]. Blondal *et al.* has validated the application of RMG-Cat in the catalytic combustion of methane on Pt(111) [34]. The operational conditions for the DR of C_2H_6 are adapted from Xie *et al.* to

validate the base results of this work [35]. As reported in the study, the flow reactor was set at 600 °C and 1 atm along with the volumetric reactant flow ratio of 1:1:2 for C_2H_6, CO_2, and Argon (as a balance).

Fig.1 shows the overall framework applied in this study, starting with the RMG simulation of the CDR on C_2H_6 according to the operating conditions mentioned above for both Pt(111) and Ni(111) surfaces with the maximal retention time of 0.05 s (pre-fixed termination time in RMG). The RMG simulation was further carried out using other LHCs under similar operating conditions, as shown in **Table 1**. The reaction temperature (600-800 °C) and reaction pressure (1-3 atm) were chosen based on the optimum conditions reported experimentally by Xie et al. [35]. A total of 72 different combinations (18 for each LHC on both Pt(111) and Ni(111) surfaces) of simulations were conducted on RMG-Cat. Each combination was carried out in triplicate to ensure the accuracy of the results obtained alongside to reduce the noise occurrence. Such replication of result is due to the nature of rate-based algorithm that RMG adopted which it will identify the reaction that most likely occurs from a pool of potential reactions, based on the species and operating conditions initiated prior to the simulation alongside the error tolerance and termination criteria specified [21]. The best combination of LHC concerning the desired products was chosen with Technique for Order of Preference by Similarity to Ideal Solution (TOPSIS). This allows us to identify the optimum operating conditions that yield the highest CO_2 conversion and H_2 yield at a specific retention time. A variation on the ratio of CO_2 and the selected LHC was conducted to identify the resulting changes. Lastly, an analysis of the energy profile for the best LHC with the operating configuration proposed was performed.

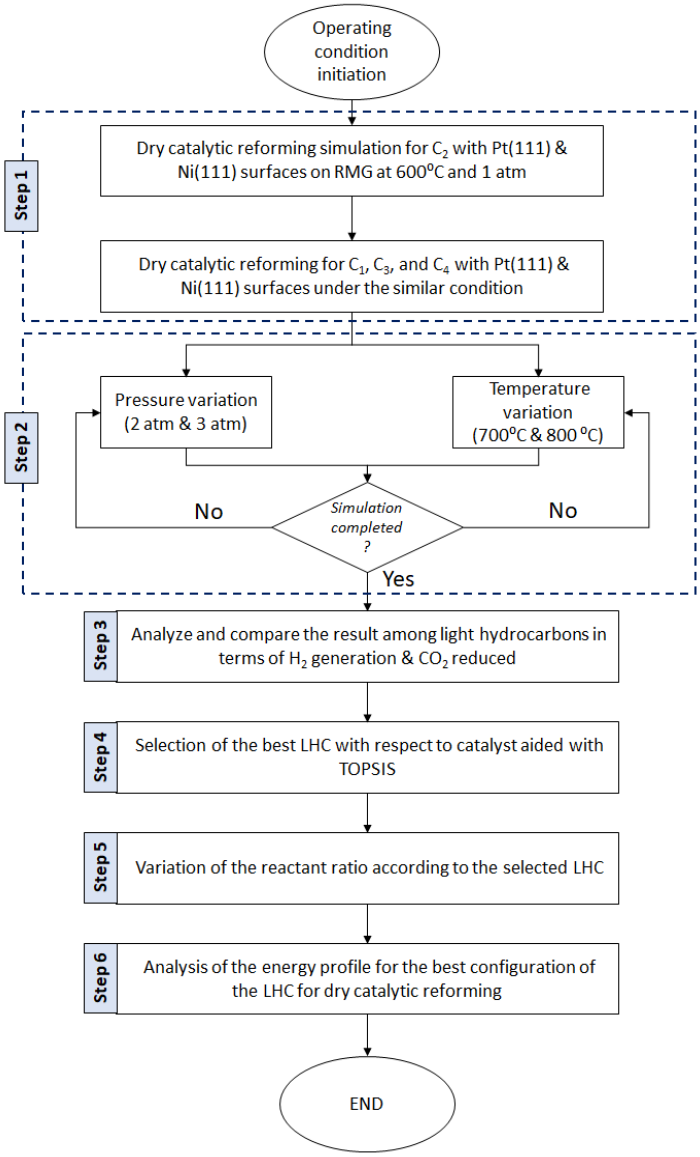

Fig. 1 Overall framework for determining the best LHC option among CH_4, C_2H_6, C_3H_8, and C_4H_{10} for H_2 generation and CO_2 utilization *via* CDR.

Table 1. Mole fraction of reactants in the CDR reaction according to the input volumetric flow rate ratio of 1:1:2 for CO_2, LHC, and Argon at a total of 40 mL/min.

Type of LHC	Input mole fraction for the reactants (mol %)		
	CO_2	LHC	Argon
Methane	0.250	0.250	0.500
Ethane	0.275	0.174	0.551
Propane	0.277	0.170	0.553
Butane	0.283	0.152	0.565

2.1 TOPSIS selection for best LHC

Technique for Order of Preference by Similarity to Ideal Solution (TOPSIS) is a multi-criteria decision method that aims to identify the potential alternatives with the nearest distance towards positive ideal solutions and most negative ideal solutions [36]. Due to its user friendly interface and high precision, it has been employed in many different applications over the years, such as in the selection of ideal solutions for the reduction in net carbon emissions [37], selection of optimal technology for Power-to-X system (transformation of municipal waste to energy) [38], formulating sustainable fertilizer for oil palm plantations [39] and optimization for the conversion of CO_2 to high-value products [40]. Both the assessment variables *(i)*, H_2 yield, and CO_2 reduction from each output, at each operating condition ($P_{i,LHC}$) are normalized ($P_{i,LHC}^{Norm}$) to the scale of 0 and 1 in accordance with each of the LHC inputs. Here, $P_{i,LHC}^{+}$ and $P_{i,LHC}^{-}$ represent the positive-ideal and negative-ideal values reported from the results of catalytic dry LHC reforming, as shown in Eq. (1).

$$P_{i,LHC}^{Norm} = \frac{P_{i,LHC} - P_{i,LHC}^{-}}{P_{i,LHC}^{+} - P_{i,LHC}^{-}} \qquad \text{Eq. (1)}$$

The general expression of the TOPSIS method, which ranks the solution based on the identified relative closeness, C_i (Eq. (2)) is calculated based on the L^2 distance towards positive- (Si_i^{+}) and negative- (Si_i^{-}) ideal solutions. Herein, a higher relative closeness value indicates a more desirable result, in this case the optimized operating conditions for each LHC.

$$C_i = \frac{Si_i^{-}}{Si_i^{+} + Si_i^{-}} \qquad \text{Eq. (2)}$$

Whereby, the L^2 distance towards the positive-ideal solution (Si_i^{+}), and negative-ideal solution (Si_i^{-}) is calculated according to Eq. (3) and Eq. (4), respectively.

$$Si_i^{+} = \sqrt{\sum_i \left(P_{i,LHC}^{Norm} - P_{i,LHC}^{+}\right)^2} \qquad \text{Eq. (3)}$$

$$Si_i^- = \sqrt{\sum_i \left(P_{i,LHC}^{Norm} - P_{i,LHC}^-\right)^2} \quad \text{Eq. (4)}$$

3. Results and Discussion

3.1 Base comparison among LHC

Fig. 2 shows the evolutionary behavior of CO_2 dry reforming of C_1-C_4 LHCs on (a) Ni(111) and (b) Pt(111) at 600 °C and 1 atm. As expected, in both catalytic systems, all the LHCs were fully degraded and remained thermodynamically stable at ~0.01 s, whereas in the absence of a catalyst, the LHC does not react with CO_2, although after a more extended period of reaction time (600 s) to achieve a stable equilibrium in reaction, as shown in **Fig. S1**. All the LHC molecules are relatively stable due to their large C-H bond energy and stable structure [41,42]. Additionally, as the DR reaction is inherently endothermic, it requires a high temperature to reach equilibrium and facilitate syngas production. On the other hand, the activation of the first C-H bond has been reported to be the rate-limiting step in the DR reaction, where the CH-O oxidation pathway is more favorable than C-O cleavage [43–45]. As a result, a shorter reaction time is observed when the LHC molecules break down to produce H_2 due to a lower energy barrier for C-H bond dissociation.

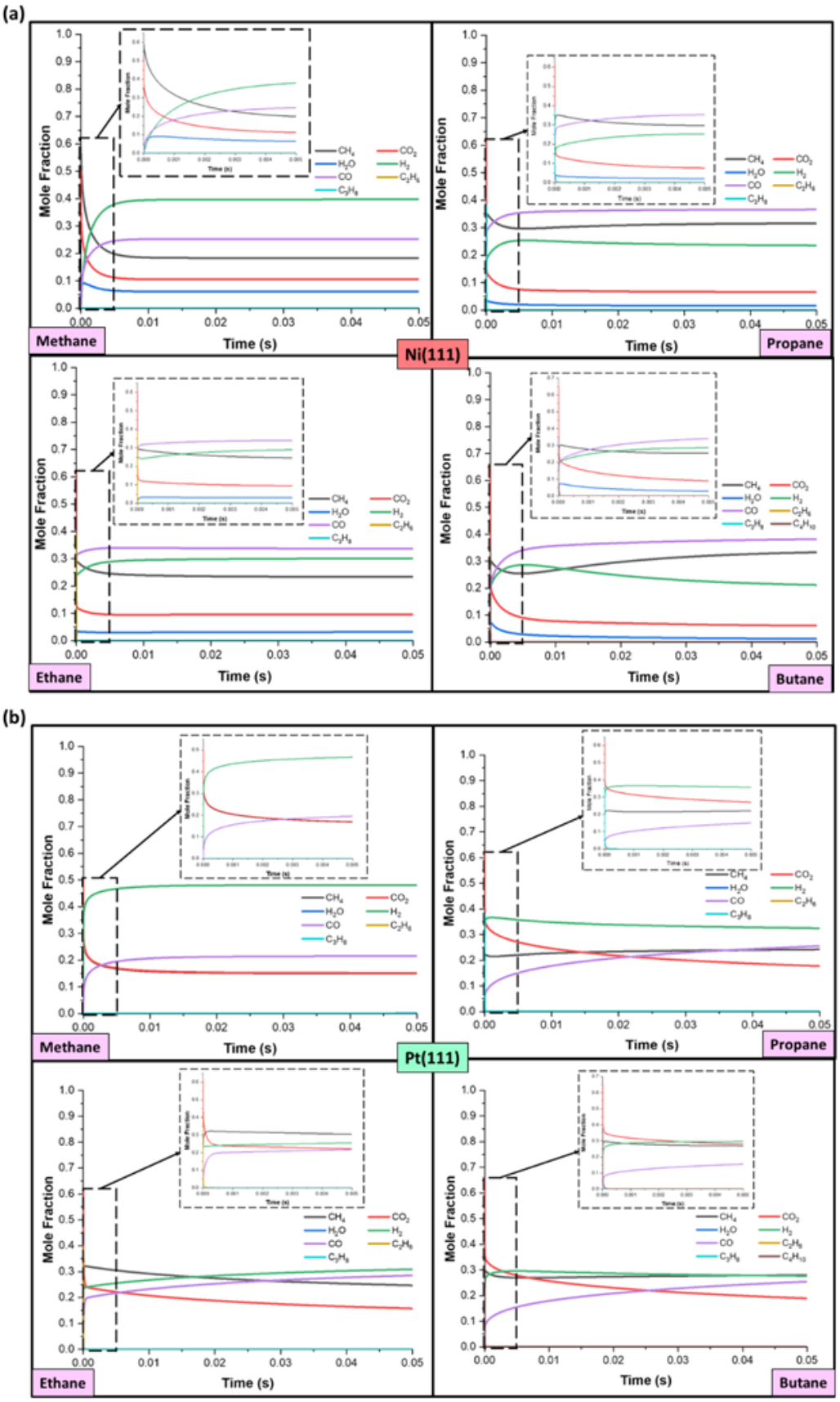
(a)
Ni(111)
Methane
Propane
Ethane
Butane
Mole Fraction
Time (s)
CH4
CO2
H2O
H2
CO
C2H4
C2H6
C4H10
(b)
Pt(111)
Methane
Propane
Ethane
Butane
Mole Fraction
Time (s)

229

Fig. 2: Evolutionary behavior of different LHC concentrations *via* CDR on (a) Ni(111) and (b) Pt(111) surfaces.

The possible reactions and products formed during the DR of LHCs in both heterogeneous and homogeneous systems are shown in **Table 2** and expressed as Eq. (5)-Eq. (30). Overall, the CDR of CH_4 is an endothermic process requiring high temperatures, > 800 °C, for complete conversion (Eq. (5)). Additionally, many possible simultaneous side reactions (e.g. water-gas shift, disproportionation, carbonization or dissociation) might happen depending on the H_2:CO ratio, as expressed in Eq. (6)-Eq. (7). Based on the thermodynamic parameter, the main DR of CH_4 (Eq. (5)) is more endothermic compared to steam reforming (Eq. (6)) and partial reforming of CH_4 (Eq. (7)), which is less feasible for long-term H_2 production. Therefore, in order facilitate DR of CH_4 on an industrial scale, an optimal catalyst must be introduced to the system to attain high conversions of CH_4 without leading to deactivation. However, the high reaction temperature for CDR of CH_4 will facilitate the simultaneous Reverse Water Gas Shift (RWGS) reaction, Eq. (14-16), which tends to reduce the H_2:CO ratio to <1 due to H_2 consumption (not favorable). The effect of the RWGS reaction can be minimized at higher reaction temperatures and/or higher ratios of CH_4:CO_2 reagents. However, higher ratios of CH_4: CO_2 (>1) have been shown to increase catalyst deactivation *via* carbon deposition [46]. The carbon formed during DRM is primarily attributed to two reactions: (i) CH_4 decomposition (Eq. (9)) and (ii) Boudouard's reaction (CO disproportionation, Eq. (13)). Meanwhile, the remaining equations (Eq. (17-26)) are dedicated to the reforming of higher carbon LHCs (C_2-C_4).

Table 2. Compilation of the possible reactions through the dry catalytic reforming of LHCs [5,12,46]

Reaction	ΔH_{298} (kJ/mol)	Equation
$CH_4 + CO_2 \leftrightarrow 2CO + 2H_2$	247.0	Eq. 5
$CH_4 + H_2O \leftrightarrow CO + 3H_2$	205.9	Eq. 6
$CH_4 + O_2 \leftrightarrow C_2H_2 + CO + H_2O$	106.0	Eq. 7
$2CH_4 + 2CO_2 \leftrightarrow C_2H_4 + 2CO + 2H_2O$	284.0	Eq. 8
$CH_4 \leftrightarrow C + 2H_2$	74.9	Eq. 9
$H_2 + CO \leftrightarrow H_2O + C$	-131.3	Eq. 10
$CO + H_2O = CO_2 + H_2$	-41.0	Eq. 11
$CO + 2H_2 \leftrightarrow CH_3OH$	-90.6	Eq. 12
$2CO \leftrightarrow C + CO_2$	-172.4	Eq. 13
$CO_2 + 2H_2 \leftrightarrow C + 2H_2O$	-90.0	Eq. 14
$CO_2 + 3H_2 \leftrightarrow CH_3OH + H_2O$	-49.1	Eq. 15
$CO_2 + 4H_2 \leftrightarrow CH_4 + 2H_2O$	-165.0	Eq. 16
$C_2H_6 + H_2O \leftrightarrow CH_4 + CO + 2H_2$	-369.7	Eq. 17
$C_2H_6 + CO_2 \leftrightarrow C_2H_4 + CO + H_2O$	-238.6	Eq. 18
$C_2H_6 \leftrightarrow C_2H_4 + H_2$	136.2	Eq. 19
$C_3H_8 + CO_2 \leftrightarrow C_3H_6 + CO + H_2O$	166.4	Eq. 20
$C_3H_8 + 6H_2O \leftrightarrow 3CO_2 + 10H_2$	374.1	Eq. 21
$C_3H_8 \rightarrow CH_4 + 2C(s) + 2H_2$	30.5	Eq. 22
$C_3H_8 + 3CO_2 \leftrightarrow 6CO + 4H_2$	620.3	Eq. 23
$C_3H_8 \rightarrow C_3H_6 + H_2$	125.0	Eq. 24
$C_3H_8 \leftrightarrow C_2H_4 + CH_4$	89.0	Eq. 25
$C_4H_{10} + H_2O \leftrightarrow C_3H_8 + CO + 2H_2$	-356.7	Eq. 26
$2CH_3OH \leftrightarrow CH_3OCH_3 + H_2O$	-37.1	Eq. 27
$CH_3OCH_3 + CO_2 \leftrightarrow 3CO + 3H_2$	258.4	Eq. 28
$CH_3OCH_3 + H_2O \leftrightarrow 2CO + 4H_2$	204.8	Eq. 29
$CH_3OCH_3 + 3H_2O \leftrightarrow 2CO_2 + 6H_2$	136.0	Eq. 30

Notably, Pt(111) was found to be more favorable towards direct dehydrogenation of CH_4 than Ni(111). This finding is in good agreement with Niu et al. [47] where they found that direct CH_4 dehydrogenation was more preferred on a Pt(111) surface. Similar observations were attained for all LHCs, where the equilibrium state was achieved in shorter reaction times, indicating a different LHC dissociation pathway for both Pt(111) and Ni(111). This finding is supported by Yan *et al.,* who found that C−C cleavage was more energetically favorable on Pt(111), whereas Ni(111) was more prone to C-O cleavage [12]. As expected, a higher syngas yield was acquired on Pt(111) compared to Ni (111), since C-C scission is the driving reaction to liberate H_2 and CO molecules **(Fig. 1).** The difference in the selectivity between Pt(111) and

Ni(111) showed that more CO is formed when using Ni(111), suggesting that reverse water gas shift reaction is promoted, whereas Pt(111) favored H_2 production. For example, CDR of C_3H_8 yielded a higher H_2 concentration on Pt(111) than Ni(111) at 600 °C at 0.325 mol% and 0.236 mol%, respectively. Additionally, the steam reforming (**Table 2**, Eq. 6, 17, 21 and 26) and WGS reactions (Eq. 11) were more favorable on Pt(111) than Ni(111) as almost all produced H_2O molecules were fully converted to H_2 and CO after ~0.01 s.

3.2 Performance across different operating conditions

3.2.1 Effect of temperature

As shown above, all the reactions presented are temperature-dependent, and large or complex molecules are less favored at high temperatures. In order to suppress the formation of large molecules such as methanol or dimethyl ether (Eq. 11- 15), a high-temperature range of 600–800 °C is more favorable. **Fig. 3(a)** and **Fig. 3(b)** illustrate the effect of reaction temperature on the H_2 yield produced from LHC on both Pt(111) and Ni(111) surfaces. An inclined temperature profile leading to a higher H_2 production can be observed among all the LHC in both catalytic surfaces. This observation is supported by Le-Chatelier's principle, in which an increase in reaction temperature for an endothermic reversible reaction would favor the forward reaction. Since most of the main reforming reactions, including DR are endothermic, an increasing temperature profile will induce a higher formation of H_2. Meanwhile, Pt(111) and Ni(111) have an immiscible two-phase system with a low mass transfer rate based on the mass transfer theory. An increase in reaction temperature can accelerate the mass transfer between the reagent molecules in the heterogeneity complex system. Thus a high kinetic energy effect can be attained in a shorter reaction time, promoting H_2 production and CO_2 conversion [48,49].

3.2.2 Effect of pressure

Based on **Fig. 3(a)** and **Fig. 3(b)** plots, it can be seen that the increase of reaction pressure was not favorable for the production of H_2 on both catalytic surfaces, regardless of the LHC used. Since most LHC–CO_2 reforming reactions are volumetric expansion processes, the reaction equilibrium conversion decreases with increased pressure in the system [50]. For instance, the CDR of C_2H_6 on Pt(111) at 600 °C showed a diminished H_2 yield from 0.309 mol% to 0.181 mol% when the pressure increased from 1 to 3 atm. A similar finding was observed for the CDR of C_2H_6 on Ni(111), the H_2 yield dropped significantly by 52.15 % when the pressure increased from 1 to 3 atm. This is due to the increase of partial pressures of each gas component within the system. Random collisions between the gas molecules on the catalytic surfaces are expected, hindering complete dissociation and dehydrogenation of C-H bonds (favoring the C-C cracking pathway). As a result, more CH* intermediates were formed, favoring the formation of alkenes such as ethylene and propene (**Table 2**, Eq. 27-30). Fig. 4(a) and Fig. 4(b) show the effect of reaction temperature and pressure on the CO_2 conversion performance for different LHCs over Pt(111) and Ni(111), respectively. From Fig. 4(a) and Fig. 4(b), it can be clearly seen that an increase in reaction pressure from 1 atm to 3 atm has improved the CO_2 conversion performance considerably regardless of the LHC, especially for Ni(111). This observation is in good agreement with the CO_2 conversion, in which the CO_2 conversion increases with higher pressure for both CDR systems. Thus, for an integrated downstream reaction that requires an H_2:CO ratio of 1 to occur, such as Fischer-Tropsch synthesis or direct synthesis of dimethyl ether (DME), a high pressure (>1 atm) is more favorable [51].

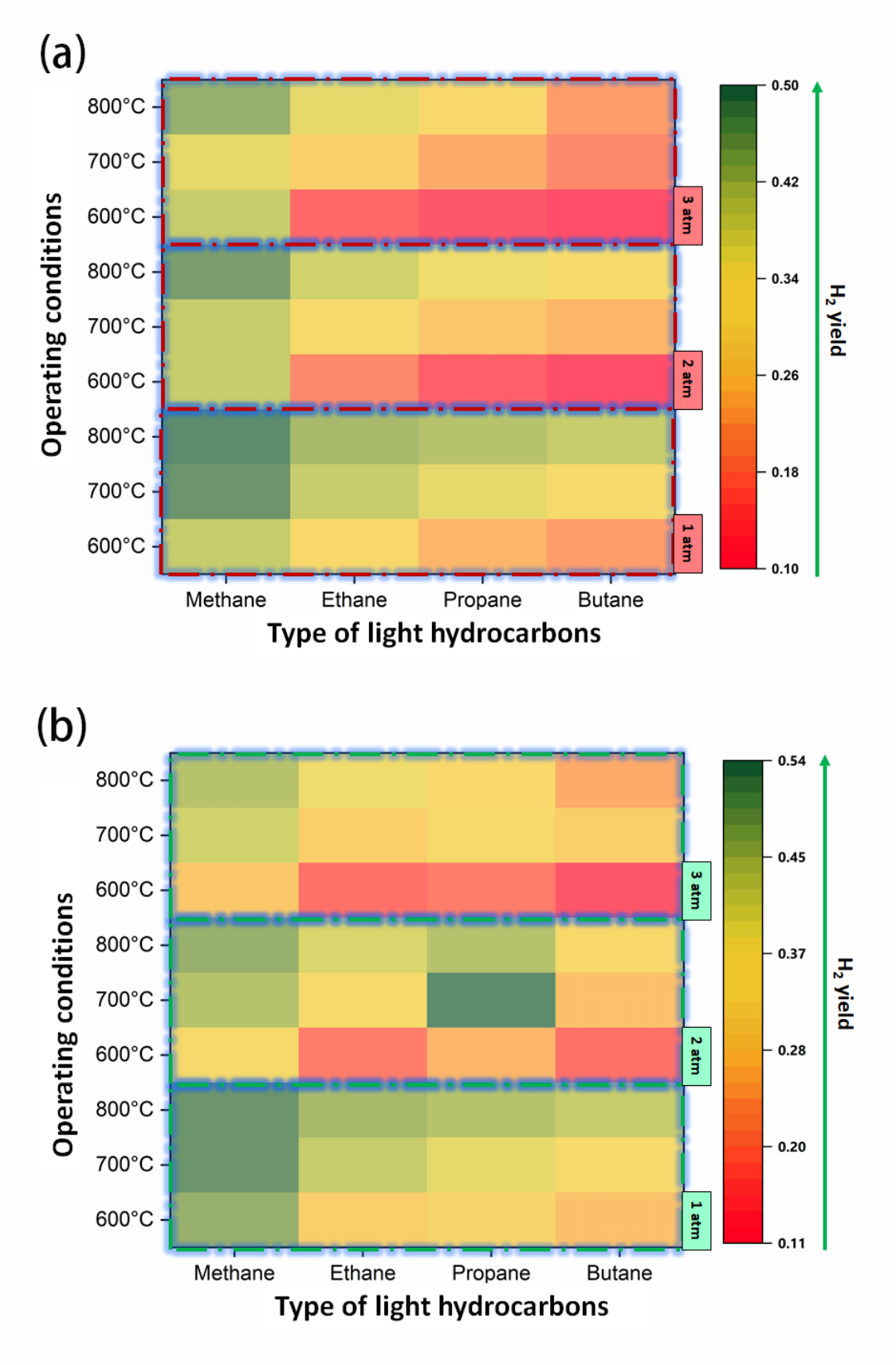

Fig. 3: H_2 yield across different operating conditions for the given LHC with a 0.05 s retention time: (a) Ni(111) and (b) Pt(111)

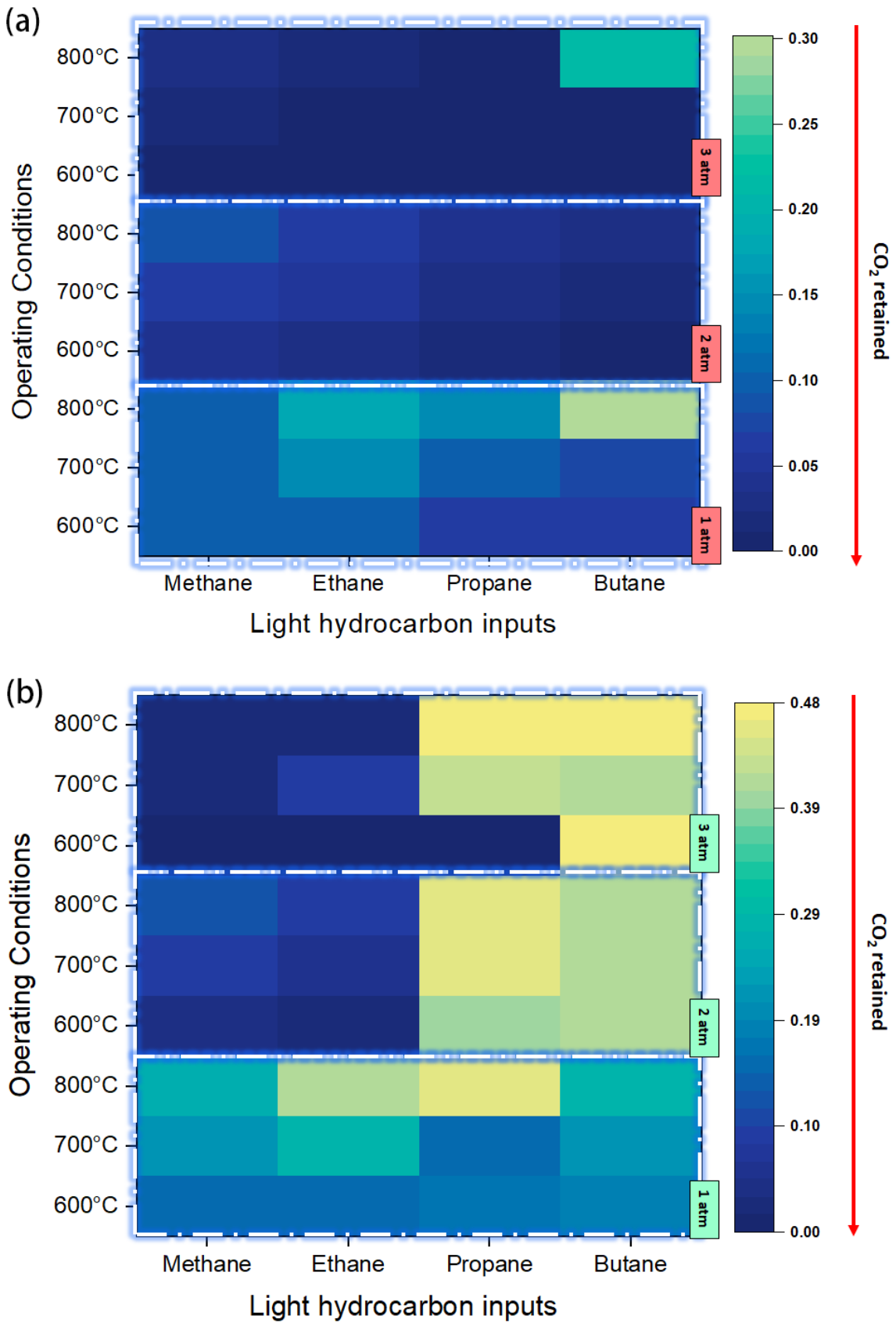

Fig. 4 Performance of CO_2 among different LHC inputs at the end of the reaction: (a) Ni(111) and (b) Pt(111)

316 *3.3 LHC reaction optimization with TOPSIS*

317 The importance of identifying the best-operating conditions for each LHC is essential
318 for a promising CO_2 conversion. Herein, TOPSIS was adopted to rank the output of each
319 operating condition for the respective LHC according to the H_2 yield and the remaining CO_2 at
320 the end of CDR, marked at 0.05 s. 0.90.90 The optimum operating conditions for C_1-C_4, by
321 considering the trade-off between the highest H_2 yield and CO_2 conversion, are shown in Fig.
322 5 according to the specified positive and negative ideal conditions. The positive ideal condition
323 indicates the output with higher H_2 yield and CO_2 converted, whereas the negative ideal
324 condition acts vice versa. The overall ranking according to the relative closeness can be referred
325 to in **Table S1** to **Table S4**. As a result, the optimum conditions for the DR of C_1 and C_2
326 hydrocarbons were 800 °C and 3 atm on Pt(111); whereas C_3 and C_4 hydrocarbons were found
327 to be favored at 800 °C and 2 atm on Ni(111) to obtain the highest H_2 yield and CO_2 conversion.
328 Although a lower pressure was found to be more favorable towards H_2 production in Section
329 3.2.2, by considering the CO_2 conversion reported, such a trade-off on achieving optimality is
330 expected. The H_2 yield and the CO_2 conversion for each LHC are summarized in **Table 3**. From
331 **Table 3**, a further ranking among the LHC was made in which the ranking sequence is
332 according to: CH_4, C_2H_6, C_4H_{10}, and C_3H_8. Therefore, one can conclude that methane is the
333 most effective in H_2 generation by utilizing CO_2 to the greatest extent due to the least energy
334 required to break down into simple molecules, as compared with other LHCs. The H_2 yield
335 was 7.3%, 10%, 12.2% higher than that of C_2H_6, C_3H_8, and C_4H_{10}, respectively on the basis of
336 the most optimum conditions.

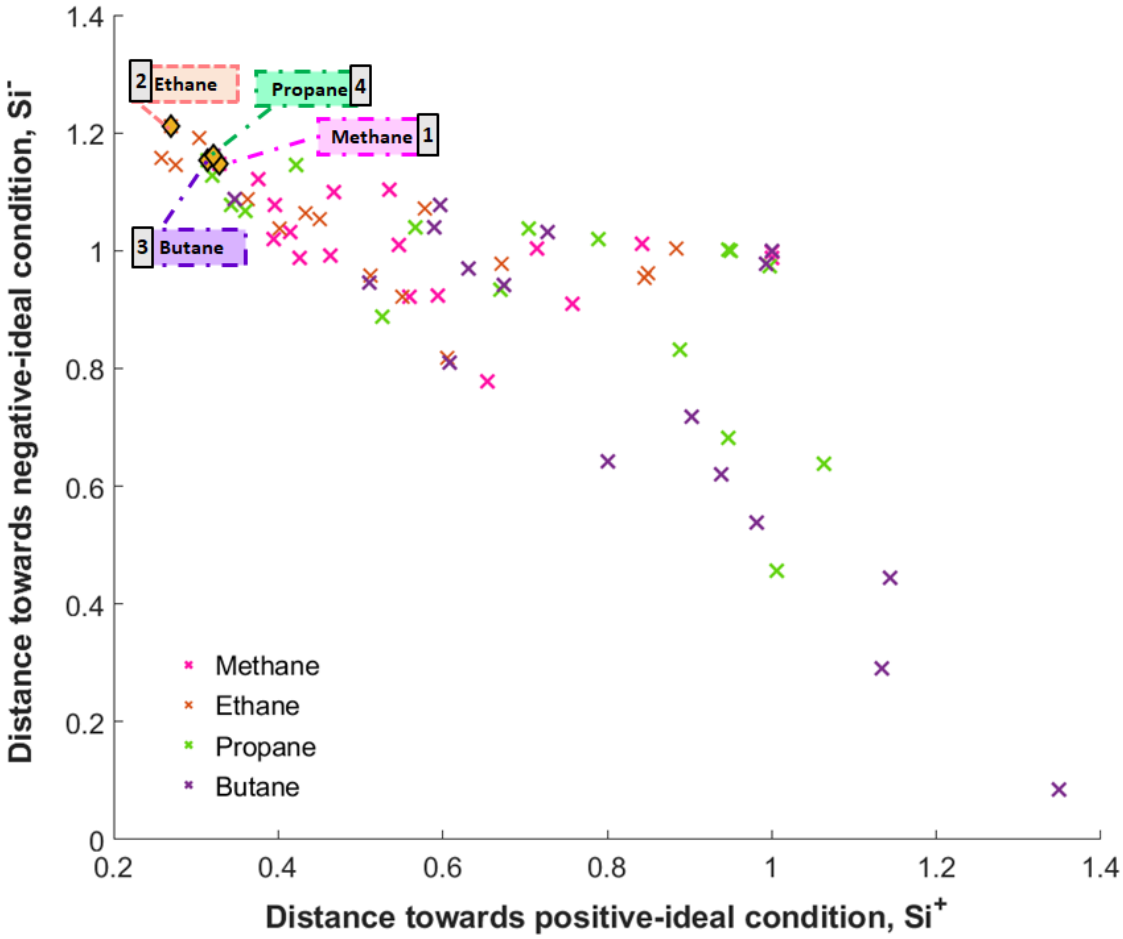

Fig. 5 Results of TOPSIS on the selection for the best operating condition combination among C_1 to C_4 LHCs according to hydrogen yield and remaining CO_2

Table 3. Hydrogen yield and CO_2 conversion of each LHC according to the best combination of operating condition

Type of LHC	Operating condition combination			Output performance		Ranking among best operating condition
	Pressure (atm)	Temperature (°C)	Catalyst	H_2 yield (mol%)	CO_2 conversion (mol%)	
Methane	3.0	800.0	Pt(111)	44.9	93.8	1
Ethane	3.0	800.0	Pt(111)	37.6	96.8	2
Propane	2.0	800.0	Ni(111)	34.9	93.4	4
Butane	2.0	800.0	Ni(111)	32.7	95.0	3

3.4 Sensitivity analysis of varying the CH_4/CO_2 ratio

The formation of coke and the occurrence of carbon deposits are not solely dependent on the reactor temperature and pressure but also on the gas inlet composition, e.g., the CH_4:CO_2 ratio, as reported by Zhang *et al.*, [52] possible aromatics such as benzene is expected with an increase of CH_4:CO_2. The concentration of ethylene and acetylene is also found to decrease slightly when increasing the CH_4:CO_2 ratio. Therefore, further investigation on the variation of the input reactant ratio towards the desired product was also conducted in this study to maximize the CO_2 utilization. The input variables of the reactant (CH_4 and CO_2), diluted in Argon spanned from a CH_4 rich stream to a CO_2 rich stream, are tabulated in **Table S6**.

As per results shown in **Fig. 6**, the H_2 yield and CO_2 reduction increased to maxima, 6.0% (Base: 44.9 mol% H_2 yields) and 5.2% (Base: 93.8 mol% CO_2 conversions), respectively at a 1:4 ratio as compared to that of a 1:1 ratio. The CH_4 conversion was reduced by 19.4% to 69.9 mol% compared to the 1:1 ratio (89.4 mol% CH_4 conversions), indicating that the CO_2 is the limiting reagent. On the other hand, the CH_4 conversion in a CO_2-rich stream was reported to be not favorable towards H_2 generation (16.7%), although a 99.9 mol% CH_4 conversion was attained. Herein, the best input reactant ratio was suggested to be 1:1 by considering the trade-off between the H_2 yield, CO_2 conversion, and CH_4 conversion, which agrees with Cao *et al* [53] which conducted a thermodynamic equilibrium analysis FactSage thermochemical software and databases. Overall, at a low CH_4:CO_2 ratio, the equilibrium in Eq. (1-4) will shift forward and thus, enhance the CO and H_2 yields. When at a high CH_4:CO_2 ratio (> 1), the CO_2 amount decreases, causing a lower CH_4 conversion. This is due to the CH_4 dissociation ($CH_4 \rightarrow C + 2H_2$) (Eq. 5), leading to coke formation on the catalyst surface. Moreover, further analysis of the input reactant (LHC/CO_2) effect on the H_2 yield, CO_2 reduction, and CH_4 conversion for other LHCs were investigated, as shown in Table S5-Table S8 and Figure S2-Figure S4.

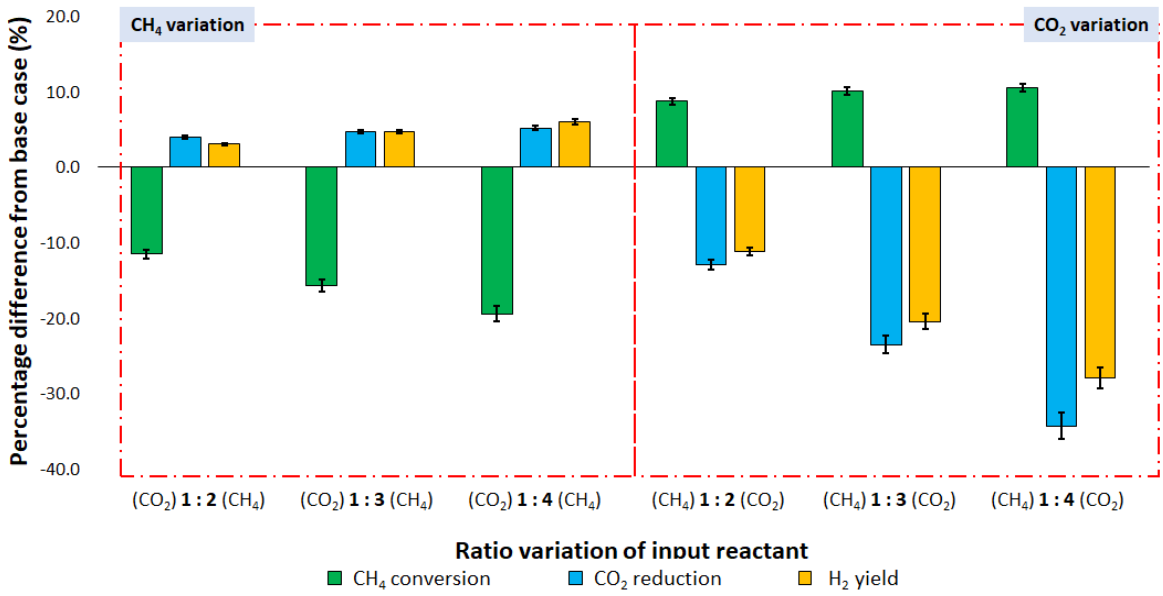

Fig. 6 Output of varying the input reactant (CO_2 and CH_4) for the dry methane reforming with Pt (111) in 3 atm, 800 °C

3.5 Energy profile and proposed mechanisms for dry reforming CH_4 on Pt(111)

According to the reaction pathways determined by the RMG network (**Fig. 7**), the whole reaction network for the DR of CH_4 (reaction conditions: Pt(111) surface, 3 atm, and 800 °C) can be separated into six sections, namely CH_4 dehydrogenation, CH_4 dissociation, CO_2 dissociation, CH oxidation, C oxidation, and H_2 formation, respectively. For CH_4 dissociation (b), direct dehydrogenation and H-assisted dehydrogenation were studied. Meanwhile, for CO_2 dissociation (c), both direct dissociation and H-assisted dissociation were investigated. For CH and C oxidation (d-e), the O* and OH* assisted pathways were considered. Lastly, H_2 formation (f) was produced from the desorbed H atoms from the Pt(111) surface.

As mentioned above, CH_4 is a stable molecule owing to its strictly symmetrical structure and large C-H bond energy (+415.5 kJ/mol). Thus, the activation of the first C-H bond *via* dehydrogenation was found to be the rate-limiting step in this reforming system, which has been extensively reported [54,55]. The first activation energy (E_a) of $CH_4^* + * \leftrightarrow CH_3^* + H^*$

on Pt(111) was found to be 0.60 eV, which is still lower than that of Ni(111) (1.21 eV) [47], Cu(111) (1.88 eV) [56], and Co(0001) (0.95 eV) [57] as reported by other researchers. Meanwhile, for CH_3*, CH_2*, and CH* dehydrogenation, the activation energies were <0.60 eV, indicating that the process can proceed smoothly with a lower energy barrier than CH_4* dehydrogenation. Also, the energy barrier for CH* dehydrogenation (0.38 eV) was still much higher than CH_4*, suggesting that CH* dehydrogenation is less favorable for Pt(111), under these conditions.

Based on the O* and OH*-assisted CH_4 dissociation graph (**Fig. 7 (b)**), the O*-assisted CH_4 direct dissociation direct pathway was more favorable due to lower energy demand, compared to OH*-assisted CH_4 dehydrogenation, specifically on CH_4*, CH_2* and CH*. Moreover, based on the O*-assisted pathway, the CH_3* dehydrogenation on Pt(111) only needed to overcome an energy barrier of 0.33 eV, much less than the OH*-assisted. It was worth noting that the direct reaction "CH_2* dehydrogenation" became exothermic after CH_3* dehydrogenation. Also, the CH* was readily oxidized (0.25 eV) rather than decomposing to carbon (1.14 eV), as a result limiting coke formation on the Pt(111) surface.

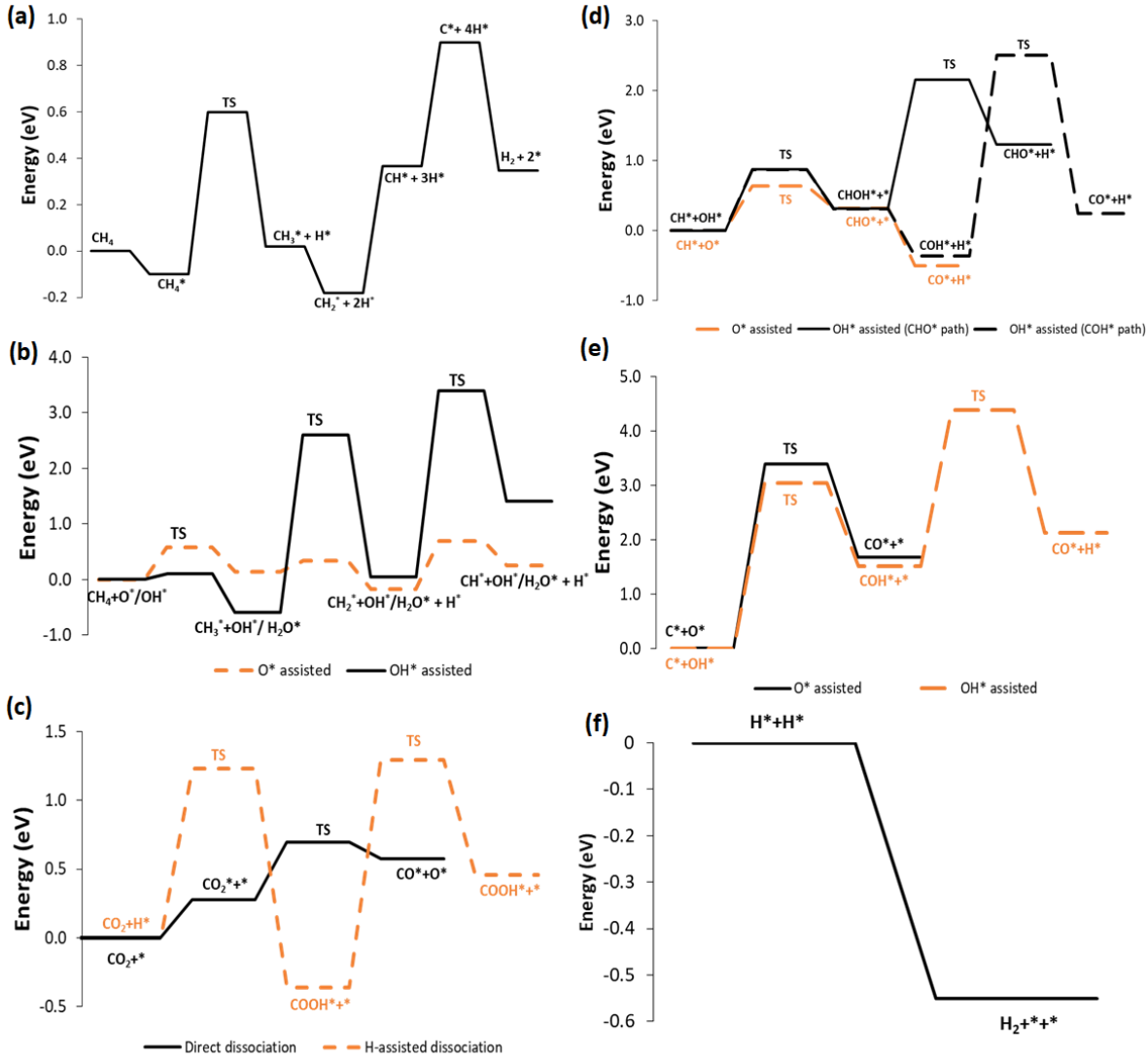

Fig. 7: Energy profile of possible reaction pathways for dry methane reforming on Pt(111) at 3 atm, 800 °C, where: (a) CH_4 direct successive dehydrogenation, (b) CH_4 dissociation through O* & OH*assisted, (c) CO_2 dissociation through direct & H-assisted, (d) CH oxidation through O* & OH* assisted, (e) C oxidation through O*& OH* assisted, and (f) H_2 formation.

For the CO_2 dissociation, the RMG simulation only considered chemisorption of CO_2* on the Pt(111) surface, **Fig. 7(c)**. Two reaction pathways were obtained, namely direct dissociation and H-assisted dissociation pathways. In general, the CO_2 can (i) directly

412 dissociate into adsorbed O and CO species on the Pt(111) surface or (ii) react with dissociated
413 H atoms and promote CO_2 hydrogenation to form an -COOH intermediate, followed by
414 continuous dissociation into adsorbed CO and OH. H-assisted dissociation was more favorable
415 from the energy profile with a lower energy barrier for the overall steps, which is in good
416 agreement with findings reported by Niu *et al.* [58]. CH oxidation is one of the crucial steps to
417 attain high CO_2 conversion and H_2 yield since they are the most abundant species in the CH_4
418 dehydrogenation process [59]. **Fig. 7(d)** shows the oxidative pathways for O*- assisted, OH*-
419 assisted (COH*), and OH*-assisted (CHO) of CH. Overall, O*- assisted CH oxidation was the
420 most favorable pathway with the lowest energy barrier of -0.5 eV as compared to its alternative
421 pathways. Meanwhile, comparing the OH*-assisted CH oxidation, the intermediate CHOH*
422 was first decomposed to CHO* or COH* at the beginning. Then, the COH* (-0.36 eV)
423 proceeds more preferentially than the CHO* pathway (1.23 eV).

424 **Fig. 7(e)** shows the energy plot of C oxidation through O*& OH* entities. The most
425 favored path was O* assisted with the activation barrier of 1.67 eV, compared to that of OH*
426 (2.12 eV). However, for the first reaction step (e.g., CO* + * and COH * + *), the energy
427 barriers attained in the COH * + * reaction was lower, indicating that OH species are more
428 effective for carbon elimination than the O species. In the last stage (H_2 formation from
429 adsorbed H atoms), the energy barrier obtained was negative with a value of -0.55 eV,
430 indicating the whole process is exothermic with no external energy required. Due to the low
431 desorption energy required, the H_2 can desorb easily from the Pt(111) surface, indicating that
432 a Pt-based catalyst is highly favorable for this reaction, illustrated in **Fig. 7(f)**.

433

434 *3.6 Thermodynamic data obtained from RMG networks*

Besides determining the most dominant pathways, the RMG simulation also provides insights into the thermodynamic of the whole system, including the enthalpy (ΔH) and Gibbs free energy (ΔG). Based on **Fig. S5** it shows that 548 reactions, out of 744 in total, had positive ΔH values, and the remaining 196 reactions had negative ΔH values at (800 °C, 3 atm on a Pt(111) surface), indicating that the overall CDR of CH_4 is an endothermic reaction system. The RMG simulation also shows that the total ΔG for the CH_4 reforming system was -303.89 eV. Based on the thermodynamic-fundamental theory, the ΔG represents the total potential energy increases in the system as the reagents are introduced and the subsequent formation of an activated complex, since the total ΔG of the system is negative at T = 800 °C, P = 3 atm. This means that the system requires a large amount of energy to react in the forward direction [60]. The reactions with the highest and lowest ΔH and ΔG were also determined by the RMG simulation (**Table 4**). The most endothermic reaction was $C_3H_3^* + H_2O^* \leftrightarrow OH^* + C_3H_4$ (218.74 kJ/mol), whereas the most exothermic reaction was $H + OH \leftrightarrow H_2O$ (-496.89 kJ/mol) in the system. This thermodynamic data can serve as a reference for engineers or researchers, bridging the existing research gap of limited fundamental microkinetic data for CDR in the literature and contribute to future decision-making for building a pilot-scale CDR plant using a Pt-based catalyst.

Table 4. Reactions reported with highest and lowest for both enthalpy and Gibbs free energy at 800 °C, 3 atm, Pt(111) surface.

Reaction	ΔH (kJ/mol)	Reaction	**ΔG (kJ/mol)**
❖ Enthalpy (Top 10 endothermic)		❖ Gibbs free energy (Top 10 non-spontaneous)	
$C_3H_3* + H_2O* \leftrightarrow OH* + C_3H_4O$	218.74	$C_3H_3* + H_2O* \leftrightarrow OH* + C_3H_4O$	235.43
$C*O* + CO_2* \leftrightarrow C_2*O_2* + O*$	184.31	$C*O* + CH_4* \leftrightarrow H* + C_2H_3O*$	185.27
$CO* + C_2H_6* \leftrightarrow CH_3* + C_2H_3O*$	167.57	$C*O* + CO_2* \leftrightarrow C_2*O_2* + O*$	181.13
$C*O* \leftrightarrow O* + C*$	162.92	$C_3H_3* + CH_4* \leftrightarrow CH_3* + C_3H_4*$	178.61
$C*O* + CH_4* \leftrightarrow H* + C_2H_3O*$	161.71	$CO* + C_2H_6* \leftrightarrow CH_3* + C_2H_3O*$	177.49
$* + C_3H_3O* \leftrightarrow C* + C_2H_3O*$	160.83	$* + C_3H_3* \leftrightarrow C* + C_2H_3*$	173.55
$C*O* + H_2O* \leftrightarrow OH* + HC*O*$	160.79	$* + C_4H_5* \leftrightarrow C* + C_3H_5*$	171.84
$CO* + H_2O* \leftrightarrow H* + HOCO*$	160.46	$C_2H_3* + H_2O* \leftrightarrow OH* + C_2H_4*$	170.08
$* + C_4H_5* \leftrightarrow C* + C_3H_5*$	157.53	$C*O* + H_2O* \leftrightarrow OH* + HC*O*$	169.95
$* + C_3H_3* \leftrightarrow C* + C_2H_3*$	155.94	$C_3H_3* + C_2H_6* \leftrightarrow C_2H_5* + C_3H_4*$	167.86
❖ Enthalpy (Top 10 exothermic)		❖ Gibbs free energy (Top 10 spontaneous)	
$H + OH \leftrightarrow H_2O$	-496.89	$H + OH \leftrightarrow H_2O$	-464.13
$CH_3* + H \leftrightarrow CH_4$	-439.61	$H + H \leftrightarrow H_2$	-406.56
$H + H \leftrightarrow H_2$	-436.01	$CHO + OH \leftrightarrow H_2O + OC$	-426.06
$CHO + OH \leftrightarrow H_2O + OC$	-430.91	$CH_3 + H \leftrightarrow CH_4$	-402.92
$C_2H_5 + H \leftrightarrow C_2H_6$	-423.04	$C_2H_5 + H \leftrightarrow C_2H_6$	-383.46
$CH_3 + OH \leftrightarrow CH_4O$	-385.93	$CHO + H \leftrightarrow H_2 + OC$	-368.53
$CH_3 + CH_3 \leftrightarrow C_2H_6$	-378.44	$CH_3 + CHO \leftrightarrow CH_4 + OC$	-364.84
$C_2H_3O + H \leftrightarrow C_2H_4O$	-374.13	$C_2H_5 + CHO \leftrightarrow C_2H_6 + OC$	-345.39
$CH_3 + CHO \leftrightarrow CH_4 + OC$	-373.59	$CH_3 + OH \leftrightarrow CH_4O$	-344.76
$C_2H_5 + CH_3 \leftrightarrow C_3H_8$	-373.25	$C_2H_5 + OH \leftrightarrow C_2H_4 + H_2O$	-341.16

4. Conclusions

An innovative and promising machine learning approach of identifying the most suitable LHC for CO_2 DR, alongside the optimum operational configuration and reaction pathways, has been proposed in this study. Based on the RMG simulation, all the possible reactions and evolutionary behavior of the CO_2 CDR for C_1-C_4 LHCs on Pt(111) and Ni(111) have been elucidated. Multiple objective optimizations across different combinations of reaction temperature and pressure for both catalytic surfaces with different LHCs were also successfully executed through TOPSIS analysis by considering the trade-off between H_2 yield and CO_2 reduction. CH4 presented the best performance among the four LHC options with the H_2 yield and CO_2 reduction of 44.9% and 93.75% at 3 atm, 800°C on a Pt (111) surface. The H_2 yields were 16.2%, 22.2%, 27.2% higher than ethane, propane, and butane, respectively (based on the most optimum conditions derived from TOPSIS analysis). Then, a sensitivity analysis on the variation of different input ratios of CH_4:CO_2 (1:1-1:4) for each LHC proposed was also executed to determine the H_2 and CO_2 reduction changes. Notably, the H_2 yield and CO_2 reduction were found to increase to 50.9 mol% and 99.0 mol%, respectively at a CH_4:CO_2 input ratio of 4:1.

Nonetheless, the reaction mechanism of the DCR of CH_4 was determined by the RMG network, the activation energy of the first C-H bond *via* dehydrogenation was found to be 0.60 eV using Pt(111), which is much lower than other catalytic surfaces reported in the literature. Also, the ranking of reactions based on the ΔH (positive to negative) and ΔG (spontaneous to non-spontaneous) from a total of 744 reforming reactions was deducted from the RMG simulation. In summary, the application of machine learning has demonstrated a great potential to be an effective and precise simulation to screen a pool of operational configuration options for possible reactions. This will reduce the time and cost associated with practical reaction optimization and provide insightful thermodynamic-microkinetic information, specifically in

the field of CO_2-assisted dry reforming of LHCs. Also, based on the optimum analysis, it is worthwhile to mention that ethane is the most potential candidate among C_2-C_4 shale gas components to substitute methane for syngas production. On a whole, similar machine learning approaches can also be applied in future thermodynamic and microkinetic works, especially for other noble and non-noble metals such as Co, Rh, Ru, Ir, Au, Ni, Cu and Fe. To further validate the accuracy and reliability of the H_2 yield and CO_2 conversion performance, confirmatory experimental can be performed over the predicted optimum reaction conditions as well.

Acknowledgment

This work was supported by a National Research Foundation (NRF) grant funded by the Korea government (MSIT) (No.2021R1A2C2007838). A.C.M. Loy would also like to acknowledge the "Australian Government Research Training Program" for supporting this project.

References

[1] S. Alataş, Res. Transp. Econ. (2021) 101047.

[2] A. Yamamoto, T. Shinkai, A.C.M. Loy, M. Mohamed, F.H.B. Baldovino, S. Yusup, A.T. Quitain, T. Kida, Sensors Actuators B Chem. 315 (2020) 128105.

[3] M. Akri, S. Zhao, X. Li, K. Zang, A.F. Lee, M.A. Isaacs, W. Xi, Y. Gangarajula, J. Luo, Y. Ren, Y.T. Cui, L. Li, Y. Su, X. Pan, W. Wen, Y. Pan, K. Wilson, L. Li, B. Qiao, H. Ishii, Y.F. Liao, A. Wang, X. Wang, T. Zhang, Nat. Commun. 10 (2019) 1–10.

[4] D. Pakhare, J. Spivey, Chem. Soc. Rev. 43 (2014) 7813–7837.

[5] J.-M. Lavoie, Front. Chem. 2 (2014) 81.

[6] Z. Sun, D.Y. Lu, R.T. Symonds, R.W. Hughes, Chem. Eng. J. 401 (2020) 123481.

[7] H. Zhang, X. Li, F. Zhu, K. Cen, C. Du, X. Tu, Chem. Eng. J. 310 (2017) 114–119.

[8] W.O. Alabi, K.O. Sulaiman, H. Wang, Chem. Eng. J. 390 (2020) 124486.

[9] V.I. Savchenko, Y.S. Zimin, A. V Nikitin, I. V Sedov, V.S. Arutyunov, J. CO2 Util. 47 (2021) 101490.

[10] R.K. Parsapur, S. Chatterjee, K.-W. Huang, ACS Energy Lett. 5 (2020) 2881–2885.

[11] A.D.N. Kamkeng, M. Wang, J. Hu, W. Du, F. Qian, Chem. Eng. J. 409 (2021) 128138.

[12] B. Yan, X. Yang, S. Yao, J. Wan, M. Myint, E. Gomez, Z. Xie, S. Kattel, W. Xu, J.G. Chen, ACS Catal. 6 (2016) 7283–7292.

[13] I. V Yentekakis, P. Panagiotopoulou, G. Artemakis, Appl. Catal. B Environ. (2021) 120210.

[14] M. Usman, W.M.A. Wan Daud, H.F. Abbas, Renew. Sustain. Energy Rev. 45 (2015) 710–744.

[15] T. Wurzel, S. Malcus, L. Mleczko, Chem. Eng. Sci. 55 (2000) 3955–3966.

[16] S. Arora, R. Prasad, RSC Adv. 6 (2016) 108668–108688.

[17] D. Xiang, P. Li, X. Yuan, H. Cao, L. Liu, Y. Liu, Appl. Therm. Eng. 193 (2021) 116990.

[18] J. Martinez-Gomez, F. Nápoles-Rivera, J.M. Ponce-Ortega, M.M. El-Halwagi, Appl. Therm. Eng. 110 (2017) 678–685.

[19] C.F. Goldsmith, R.H. West, J. Phys. Chem. C 121 (2017) 9970–9981.

[20] G.R. Wittreich, K. Alexopoulos, D.G. Vlachos, Handb. Mater. Model. Appl. Curr. Emerg. Mater. (2020) 1377–1404.

[21] C.W. Gao, J.W. Allen, W.H. Green, R.H. West, Comput. Phys. Commun. 203 (2016) 212–225.

[22] R. Van De Vijver, N.M. Vandewiele, P.L. Bhoorasingh, B.L. Slakman, F.S. Khanshan, H.H. Carstensen, M.F. Reyniers, G.B. Marin, R.H. West, K.M. Van Geem, Int. J. Chem. Kinet. 47 (2015) 199–231.

[23] J. Hu, P. Hongmanorom, V. V Galvita, Z. Li, S. Kawi, Appl. Catal. B Environ. 284 (2021) 119734.

[24] M.E.S. Hegarty, A.M. O'Connor, J.R.H. Ross, Catal. Today 42 (1998) 225–232.

[25] P.O. Graf, B.L. Mojet, L. Lefferts, Appl. Catal. A Gen. 346 (2008) 90–95.

[26] L.C.P.F. Júnior, S. de Miguel, J.L.G. Fierro, M. do Carmo Rangel, in: F. Bellot Noronha, M. Schmal, E.B.T.-S. in S.S. and C. Falabella Sousa-Aguiar (Eds.), Nat. Gas Convers. VIII, Elsevier, 2007, pp. 499–504.

[27] Z. Liu, F. Zhang, N. Rui, X. Li, L. Lin, L.E. Betancourt, D. Su, W. Xu, J. Cen, K. Attenkofer, H. Idriss, J.A. Rodriguez, S.D. Senanayake, ACS Catal. 9 (2019) 3349–3359.

[28] N.A.K. Aramouni, J.G. Touma, B.A. Tarboush, J. Zeaiter, M.N. Ahmad, Renew. Sustain. Energy Rev. 82 (2018) 2570–2585.

[29] I. V Yentekakis, G. Goula, M. Hatzisymeon, I. Betsi-Argyropoulou, G. Botzolaki, K. Kousi, D.I. Kondarides, M.J. Taylor, C.M.A. Parlett, A. Osatiashtiani, G. Kyriakou, J.P. Holgado, R.M. Lambert, Appl. Catal. B Environ. 243 (2019) 490–501.
[30] W.H. Green, R.H. West, (n.d.).
[31] F. Seyedzadeh Khanshan, R.H. West, Fuel 163 (2016) 25–33.
[32] N. Mimura, I. Takahara, M. Inaba, M. Okamoto, K. Murata, Catal. Commun. 3 (2002) 257–262.
[33] M.D. Porosoff, M.N.Z. Myint, S. Kattel, Z. Xie, E. Gomez, P. Liu, J.G. Chen, Angew. Chemie - Int. Ed. 54 (2015) 15501–15505.
[34] K. Blondal, J. Jelic, E. Mazeau, F. Studt, R.H. West, C.F. Goldsmith, Ind. Eng. Chem. Res. 58 (2019) 17682–17691.
[35] Z. Xie, B. Yan, J.H. Lee, Q. Wu, X. Li, B. Zhao, D. Su, L. Zhang, J.G. Chen, Appl. Catal. B Environ. 245 (2019) 376–388.
[36] C.-L. Hwang, K. Yoon, in: C.-L. Hwang, K. Yoon (Eds.), Springer Berlin Heidelberg, Berlin, Heidelberg, 1981, pp. 58–191.
[37] L. Li, Z. Yao, S. You, C.-H. Wang, C. Chong, X. Wang, Appl. Energy 243 (2019) 233–249.
[38] M.A. Alao, T.R. Ayodele, A.S.O. Ogunjuyigbe, O.M. Popoola, Energy 201 (2020) 117675.
[39] J.Y. Lim, B.S. How, S.Y. Teng, W.D. Leong, J.P. Tang, H.L. Lam, C.K. Yoo, Resour. Conserv. Recycl. 166 (2021) 105357.
[40] K.A. Pacheco, A.E. Bresciani, R.M.B. Alves, J. CO2 Util. 43 (2021) 101391.
[41] H.S. Truong-Lam, S. Seo, S. Kim, Y. Seo, J.D. Lee, Energy & Fuels 34 (2020) 6288–6297.
[42] H. Schwarz, Angew. Chemie - Int. Ed. 50 (2011) 10096–10115.
[43] C.C. Chang, C.Y. Liu, S.Y. Wu, M.K. Tsai, Phys. Chem. Chem. Phys. 19 (2017) 4989–4996.
[44] M.L. Yang, Y.A. Zhu, C. Fan, Z.J. Sui, D. Chen, X.G. Zhou, Phys. Chem. Chem. Phys. 13 (2011) 3257–3267.
[45] J. Wei, E. Iglesia, J. Catal. 224 (2004) 370–383.
[46] T. Schaaf, J. Grünig, M.R. Schuster, T. Rothenfluh, A. Orth, Energy. Sustain. Soc. 4 (2014) 2.
[47] J. Niu, J. Ran, D. Chen, Appl. Surf. Sci. 513 (2020) 145840.
[48] A.C.M. Loy, A.T. Quitain, M.K. Lam, S. Yusup, M. Sasaki, T. Kida, Energy Convers. Manag. 180 (2019) 1013–1025.
[49] I. Izhab, M. Asmadi, N.A. Saidina Amin, Int. J. Hydrogen Energy (2020).
[50] Y. Zhang, G. Zhang, B. Zhang, F. Guo, Y. Sun, Chem. Eng. J. 173 (2011) 592–597.
[51] V. Dieterich, A. Buttler, A. Hanel, H. Spliethoff, S. Fendt, Energy Environ. Sci. 13 (2020) 3207–3252.
[52] D. Zhang, M. Yang, X. Feng, Y. Wang, ACS Sustain. Chem. Eng. 8 (2020) 11376–11388.
[53] P. Cao, S. Adegbite, T. Wu, Energy Procedia 105 (2017) 1864–1869.
[54] E. Gomez, S. Kattel, B. Yan, S. Yao, P. Liu, J.G. Chen, Nat. Commun. 9 (2018) 1398.
[55] S.-G. Wang, D.-B. Cao, Y.-W. Li, J. Wang, H. Jiao, J. Phys. Chem. B 110 (2006) 9976–9983.
[56] H. Liu, R. Zhang, R. Yan, J. Li, B. Wang, K. Xie, Appl. Surf. Sci. 258 (2012) 8177–8184.
[57] H. Huang, Y. Yu, M. Zhang, Phys. Chem. Chem. Phys. 22 (2020) 27320–27331.
[58] J. Niu, Y. Wang, Y. Qi, A.H. Dam, H. Wang, Y.-A. Zhu, A. Holmen, J. Ran, D. Chen, Fuel 266 (2020) 117143.

[59] Q. Qi, X. Wang, L. Chen, B. Li, Appl. Surf. Sci. 284 (2013) 784–791.
[60] A.C.M. Loy, D.K.W. Gan, S. Yusup, B.L.F. Chin, M.K. Lam, M. Shahbaz, P. Unrean, M.N. Acda, E. Rianawati, Bioresour. Technol. 261 (2018) 213–222.